Hindawi Publishing Corporation
Journal of Nanomaterials
Volume 2016, Article ID 5837406, 8 pages
http://dx.doi.org/10.1155/2016/5837406

Research Article

Ag-Decorated Fe_3O_4@SiO_2 Nanorods: Synthesis, Characterization, and Applications in Degradation of Organic Dyes

Chao Li, Junjie Sun, Duo Chen, Guangbing Han, Shuyun Yu, Shishou Kang, and Liangmo Mei

School of Physics and National Key Laboratory of Crystal Materials, Shandong University, Jinan 250100, China

Correspondence should be addressed to Shishou Kang; skang@sdu.edu.cn

Received 7 March 2016; Accepted 20 April 2016

Academic Editor: Federico Cesano

Well-dispersed Ag nanoparticles (NPs) are successfully decorated on Fe_3O_4@SiO_2 nanorods (NRs) via a facile step-by-step strategy. This method involves coating α-Fe_2O_3 NRs with uniform silica layer, reduction in 10% H_2/Ar atmosphere at 450°C to obtain Fe_3O_4@SiO_2 NRs, and then depositing Ag NPs on the surface of Fe_3O_4@SiO_2 NRs through a sonochemical step. It was found that the as-prepared Ag-decorated magnetic Fe_3O_4@SiO_2 NRs (Ag-MNRs) exhibited a higher catalytic efficiency than bare Ag NPs in the degradation of organic dye and could be easily recovered by convenient magnetic separation, which show great application potential for environmental protection applications.

1. Introduction

With the development of modern industry, water pollution due to the immoderate discharge of organic contaminants, especially organic dyes, has become one of the major environmental issues. Various kinds of treatment schemes have been exploited to deal with these effluents, such as polymer adsorption, photocatalytic degradation, and noble metal catalytic reduction [1–3]. Among these methods, noble metal (e.g., Au, Pt, Pd, and Ag) nanoparticles (NPs) based catalysts have received significant attention due to their excellent catalytic activity and efficiency [3–6]. As a relatively low-cost noble material, Ag NPs have attracted particularly interest for their remarkably catalytic/antibacterial activity [7, 8]. However, there are two obvious disadvantages which may hinder the further practical applications of Ag NPs in industry. On one hand, Ag NPs are difficult to remove from the solution systems by simple centrifugation or filtration routes after the reaction due to their small size, which may lead to the secondary pollution and resource waste. On the other hand, pure Ag NPs are easy to coalesce with each other during the synthesis and catalytic process owing to their high surface energy, which will cause a fast drop of the catalytic activity and stability. A normal solving method is to immobilize and graft the NPs onto inorganic supports, such as polystyrene silica, carbon, and magnetic NPs to form a core/shell nanostructure [9–11]. Among these supports, Fe_3O_4@SiO_2 nanocomposites (NCs) have long been employed as promising supports to enhance the dispersion and recovery of Ag based catalysts [12, 13]. The Fe_3O_4@SiO_2 NCs can be easily recovered by magnetic separation, and the silica shell coated outside the Fe_3O_4 NPs supplies not only a protection for the magnetic core from corrosion but also a suitable supporting matrix to incorporate other functional materials.

For a well-defined core/shell nanostructure, synergistic effects between the core and shell part are important for promoting their operational performance [14]. Apart from the size and composition, shape and morphology could also significantly influence their practical properties. Previously researches have shown that high aspect ratio nanostructures (e.g., ellipsoidal particles) may present higher catalytic rate than low aspect ratio nanostructures in heterogeneous catalysis systems [15, 16]. However, most of the Fe_3O_4@SiO_2 supports used in metal based catalysts were spheres or

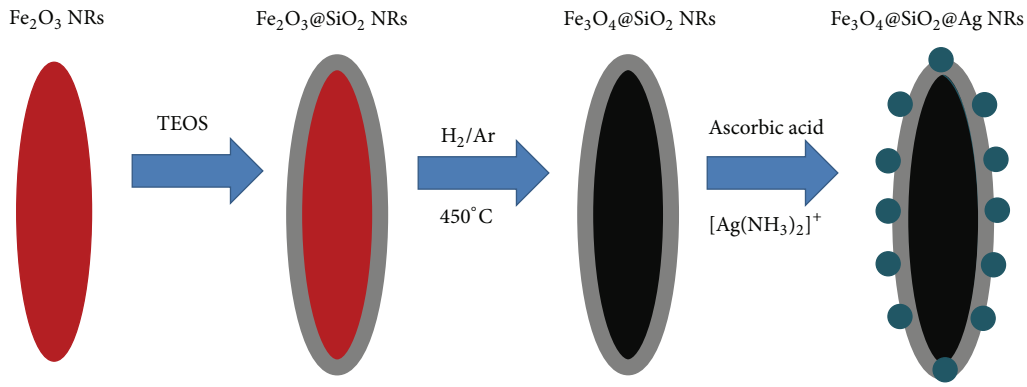

FIGURE 1: Schematic illustration for the preparation of the Ag-decorated Fe_3O_4@SiO_2 NRs.

cubes [8, 12, 17, 18]; rare reports were focused on the anisotropic nanostructures. In this letter, we develop a facile step-by-step route to deposit well-dispersed Ag NPs on Fe_3O_4@SiO_2 nanorods (NRs) for the first time. The composition, structure, and magnetic properties of the as-prepared Ag-decorated magnetic Fe_3O_4@SiO_2 NRs (Ag-MNRs) were investigated, respectively. These nanostructures exhibited remarkably catalytic efficiency for the degradation of organic dyes and showed a superior recyclability.

2. Experiment

2.1. Synthesis of α-Fe_2O_3@SiO_2 NRs. For the preparation of α-Fe_2O_3@SiO_2 NRs, α-Fe_2O_3 NRs were first synthesized through a modified hydrothermal method previously reported [19]. Typically, specific amounts of ferric chloride (0.02 M) and ammonium dihydrogen phosphate (0.7 mM) were added into deionized water (40 mL) and stirred for 15 min. The mixture was then transferred into Teflon-lined stainless-steel autoclave (50 mL) and sealed at 220°C for 40 h. After the autoclave cooled down to room temperature, the precipitates were centrifuged and washed with deionized water. The silica shell was coated according to the literature [20]. Simply, the as-prepared α-Fe_2O_3 NRs were dispersed into a solution containing water (20 mL), absolute ethanol (160 mL), tetraethoxysilane (60 μL), and ammonia hydroxide (5 mL) and stirred for 6 h. The particles were collected by centrifugation and washed with absolute ethanol.

2.2. Fe_3O_4@SiO_2 NRs. The products obtained above were calcined at 450°C in 10% H_2/Ar atmosphere for 5 h; after the annealing process, the α-Fe_2O_3@SiO_2 NRs were completely transformed into Fe_3O_4@SiO_2 NRs.

2.3. Preparation of Ag-MNRs. The obtained Fe_3O_4@SiO_2 NRs (10 mg) were added into $[Ag(NH_3)_2]^+$ aqueous solution (30 mL, 0.01 M) and ultrasonicated for 30 min. After that, Ascorbic Acid aqueous solution (2 mL, 0.05 M) was injected into the mixture drop by drop and ultrasonicated for another 30 min. The products were separated using a magnet, purified with deionized water and absolute ethanol, and dried at 50°C for 12 h. Bare Ag NPs were prepared in a similar way without adding magnetic supports.

2.4. Catalytic Performance Measurement

2.4.1. Reduction of Rhodamine B (RhB). To evaluate the catalytic activity of Ag-MNRs, sodium borohydride aqueous solution (2 mL, 0.15 M) was added into RhB aqueous solution (20 mL, 0.0625 mM) under stirring. Subsequently, certain amounts of Ag-MNRs (2 mg, 3 mg, and 4 mg) were dispersed in the above solution at room temperature. Changes of the absorption peak at 553 nm in UV-Vis spectrometer were recorded. A similar way was applied for evaluating the catalytic ability of Fe_3O_4@SiO_2 NRs and bare Ag NPs.

2.4.2. Reduction of Methyl Blue (MB). Sodium borohydride aqueous solution (2 mL, 0.15 M) was added into MB aqueous solution (20 mL, 0.0415 mM) under stirring. Subsequently, Ag-MNRs (4 mg) were dispersed in the above solution at room temperature. Changes of the absorption peak at 660 nm in UV-Vis spectrometer were recorded.

2.5. Characterizations. The crystalline structure was investigated by X-ray power diffraction (Bruker D8 ADVANCE). The transmission electron microscopy (TEM) and high-resolution transmission electron microscopy (HRTEM) were conducted on JEM 1200EX microscope operated at 200 kV. Element analysis was taken on a S-4800 scanning electron microscope. X-ray photoelectron spectroscopy (XPS) analysis was performed on Thermo ESCALAB 250Xi. The Ultraviolet-visible (UV-Vis) spectroscopy measurements were recorded on a F-4500 ultraviolet-visible spectrophotometer. The magnetic properties of the products were measured by alternative gradient magnetometer (2900-04C).

3. Results and Discussion

The fabrication procedure of the Ag-MNRs is schematically illustrated in Figure 1. Monodispersed α-Fe_2O_3 NRs were synthesized firstly via a hydrothermal route, followed by coating with silica layer through the hydrolysis and condensation of TEOS. The products were then calcined in

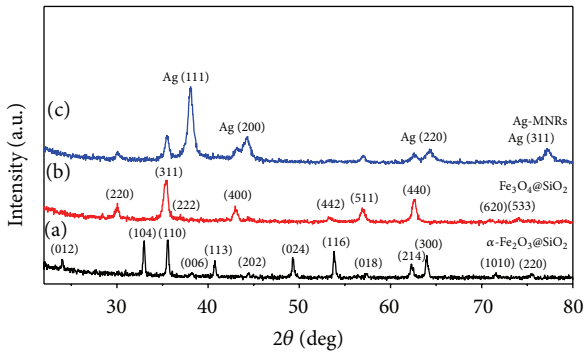

FIGURE 2: XRD patterns of synthesized (a) α-Fe_3O_4@SiO_2 NRs, (b) Fe_3O_4@SiO_2 NRs, and (c) Ag-MNRs.

reduction atmosphere which transformed the nonmagnetic α-Fe_2O_3@SiO_2 NRs into magnetic Fe_3O_4@SiO_2 NRs. After that, Ag NPs were deposited on the surface of the magnetic Fe_3O_4@SiO_2 NRs through a sonochemical step and the Ag-MNRs were obtained.

The phase purity and composition of the products were investigated by XRD measurements. Figure 2(a) shows XRD pattern of the α-Fe_2O_3@SiO_2 NRs, compared with the data in JCPDS number 871165; all peaks in the pattern can be indexed to trigonal α-Fe_2O_3. After annealing in reduction atmosphere, the phase was completely transformed to cubic Fe_3O_4 (JCPDS number 75-1609, Figure 2(b)). No other peaks are observed in both Figures 2(a) and 2(b), suggesting an amorphous character of the silica layer. In the case of Ag-MNRs (Figure 2(c)), besides the diffraction peaks of Fe_3O_4, several additional peaks centered at $2\theta = 38.2^\circ$, 44.4°, 64.6°, and 77.5° can be attributed to the (111), (200), (220), and (311) crystal planes of metallic Ag (JCPDS number 87-0720). The sharp diffraction peaks indicate that highly crystallized Ag NPs have been successfully decorated on the Fe_3O_4@SiO_2 NRs.

The morphology and structure of the samples were investigated by TEM and HRTEM. As shown in Figure 3(a), the average length and diameter of the α-Fe_2O_3@SiO_2 NRs are about 450±20 nm and 90±20 nm, respectively. The surface of the α-Fe_2O_3 NRs was fully coated with a smooth SiO_2 layer whose average thickness is about 8 nm. Figure 3(b) reveals that the one-dimensional structure was still maintained after the thermal treatment, and this could be attributed to the presence of SiO_2 shell which may act as space barrier. The d-spacing of the crystallized magnetic core is about 0.294 nm (inset in Figure 3(b)), which is consistent with the (220) plane in cubic magnetite crystal.

Figure 3(c) shows the TEM image of Ag-MNRs. It can be clearly seen that highly dispersed Ag NPs were decorated on the surface of Fe_3O_4@SiO_2 NRs. HRTEM image inset in Figure 3(c) shows lattice fringes with a spacing of about 0.236 nm, which is consistent with the Ag (111) plane spacing. The size distribution of Ag NPs is quite narrow with an average size of 7.63 nm (Figure 3(d)), indicating that this method exhibits a good control on the fabrication of Ag NPs.

EDS and XPS measurements were carried out to further confirm the composition and surface chemical state of the Ag-MNRs. Figure 4(a) depicts the existence of Ag, Fe, Si, and O in the Ag-MNRs, and the percentage of Ag in the Ag-MNRs is about 20.88%. Figure 4(b) shows the Ag 3d core level spectrum; the banding energies centered at 367.6 eV and 373.6 eV with a difference of 6 eV are corresponding to Ag $3d_{5/2}$ and Ag $3d_{3/2}$ peaks, respectively, indicating metallic Ag in the Ag-MNRs [21].

RhB was selected as a model organic dye to evaluate the catalytic performance of the Ag-MNRs with $NaBH_4$ as reducing agent. As observed in Figure 5(a), nearly no intensity change of the peak at 553 nm was found after 1 h reduction in the absence of $NaBH_4$ or Ag-MNRs, indicating that the reduction reaction is very slow in the absence of catalyst or reducing agent. After the addition of $NaBH_4$ and Ag-MNRs, the absorption peak at 553 nm gradually decreased with reaction time (Figure 5(b)). The ability of Fe_3O_4@SiO_2 NRs and bare Ag NPs to catalyze the reduction of RhB were also tested and compared to the result of Ag-MNRs. Figure 5(c) shows the kinetic curves for the reduction of RhB by Ag-MNRs, bare Ag NPs, and Fe_3O_4@SiO_2 NRs. The linear variation of $\ln(C_t/C_0)$ versus reaction time indicates that the reaction follows first-pseudo-order kinetics [22–24], where C_0 and C_t represent the concentration of the RhB after time 0 and t min reaction. According to the formula $\ln(C_t/C_0) = -kt$, the apparent rate constants k (min^{-1}) estimated from the slopes of straight lines are 0.152 min^{-1}, 0.039 min^{-1}, and 0.0016 min^{-1}, respectively. The Ag-MNRs show superior enhanced catalytic activity than bare Ag NPs. It can be seen that the Fe_3O_4@SiO_2 NRs do not show obvious catalytic ability toward RhB degradation, so this observed enhancement of the catalytic efficiency could be attributed to the following two reasons. (1) It is well known that catalytic activity of the metal particles comes from their ability of transferring electron from donor to acceptor [25]. The Ag NPs in Ag-MNRs exhibit better dispersibility and smaller size than bare Ag NPs, which would make the dye molecules contact with Ag NPs sufficiently and lower their interface potential barrier height [26]. Thus, the Ag NPs supported on Fe_3O_4@SiO_2 NRs show a fast electron transfer rate between the catalyst and dye molecules. (2) The rod-like structure of the catalysts provides large surface areas for adsorbing dye molecules, which lead to a high rate of reduction. In addition, the synergetic effect between Fe_3O_4@SiO_2 NRs and Ag NPs could also exert an influence for promoting the catalytic performance.

The impact of the catalyst concentration and pH value on the catalytic activity were also investigated. Figure 6(a) depicts that higher catalysts concentration results in a faster reduction rate, which is in accordance with previous studies [27, 28]. The kinetic curves for the reduction of RhB by Ag-MNRs with different pH values were shown in Figure 6(b). No obvious change on the catalytic activity was observed under different pH values, indicating that the superior catalytic ability of the Ag-MNRs could be maintained in different pH value conditions.

For further examining the catalytic universality of Ag-MNRs, MB was chosen as another target to check the catalytic ability of Ag-MNRs. Figure 7(a) shows the successive UV-Vis absorption spectra of the MB reduction solution in

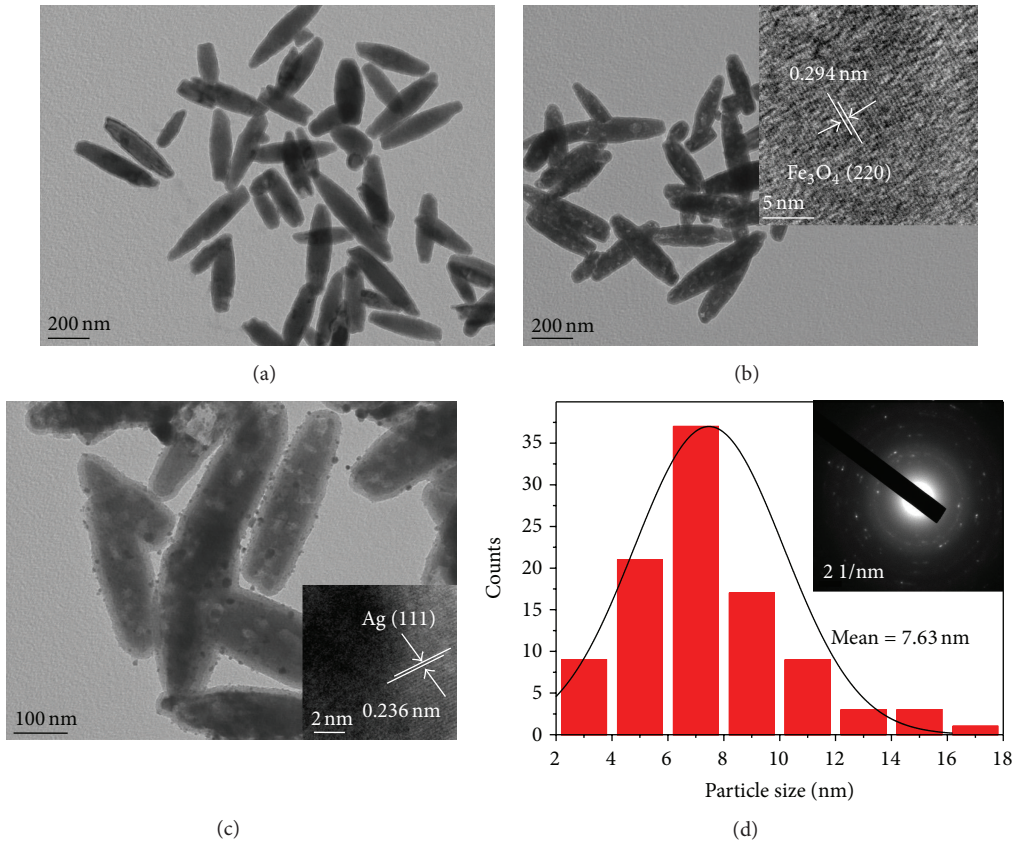

Figure 3: TEM and HRTEM images (inset Figures 3(b) and 3(c)) of (a) α-Fe_2O_3@SiO_2 NRs, (b) Fe_3O_4@SiO_2 NRs, (c) Ag-MNRs, and (d) the size distribution and SAED (inset Figure 3(d)) of Ag NPs in Ag-MNRs.

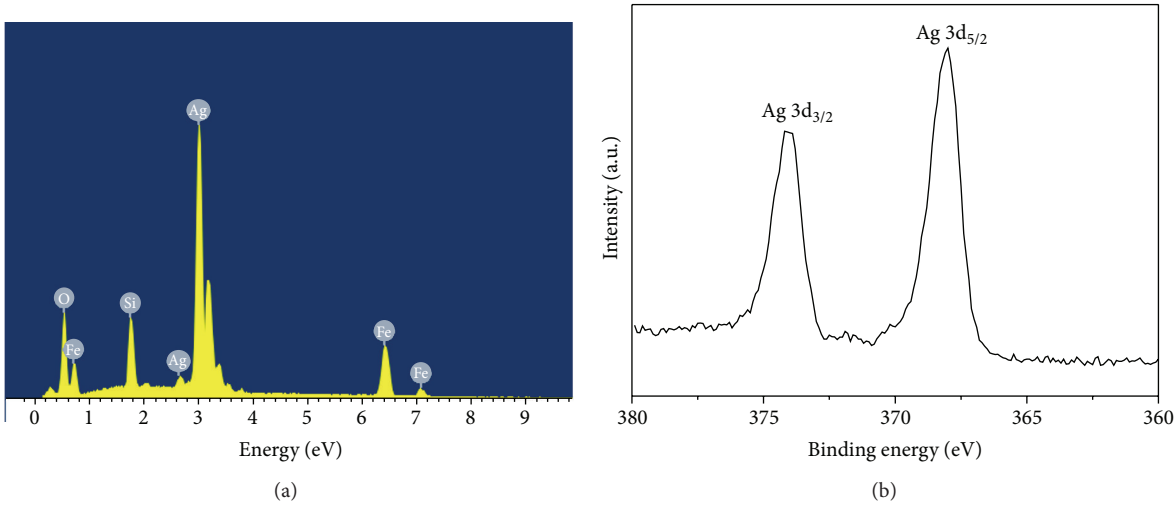

Figure 4: (a) EDS spectra of Ag-MNRs and (b) XPS spectra of Ag in Ag-MNRs.

the presence of Ag-MNRs. The intensity of the absorption peak at 665 nm decreased gradually with reaction time, indicating that the degradation of MB by using Ag-MNRs proceeded successfully. Figure 7(b) displays the kinetic curves for the reduction of MB by Ag-MNRs and the k value estimated from the slope of the straight line is 0.242 min^{-1}.

The hysteresis loops of the prepared samples (Fe_3O_4@SiO_2 NRs and Ag-MNRs.) were measured by AGM instrument at room temperature. As shown in Figure 8(a), both samples displayed typical ferromagnetic behavior. The magnetization saturation (M_s) values for Fe_3O_4@SiO_2 NRs and Ag-MNRs are 39.4 emu/g and 30.2 emu/g, respectively.

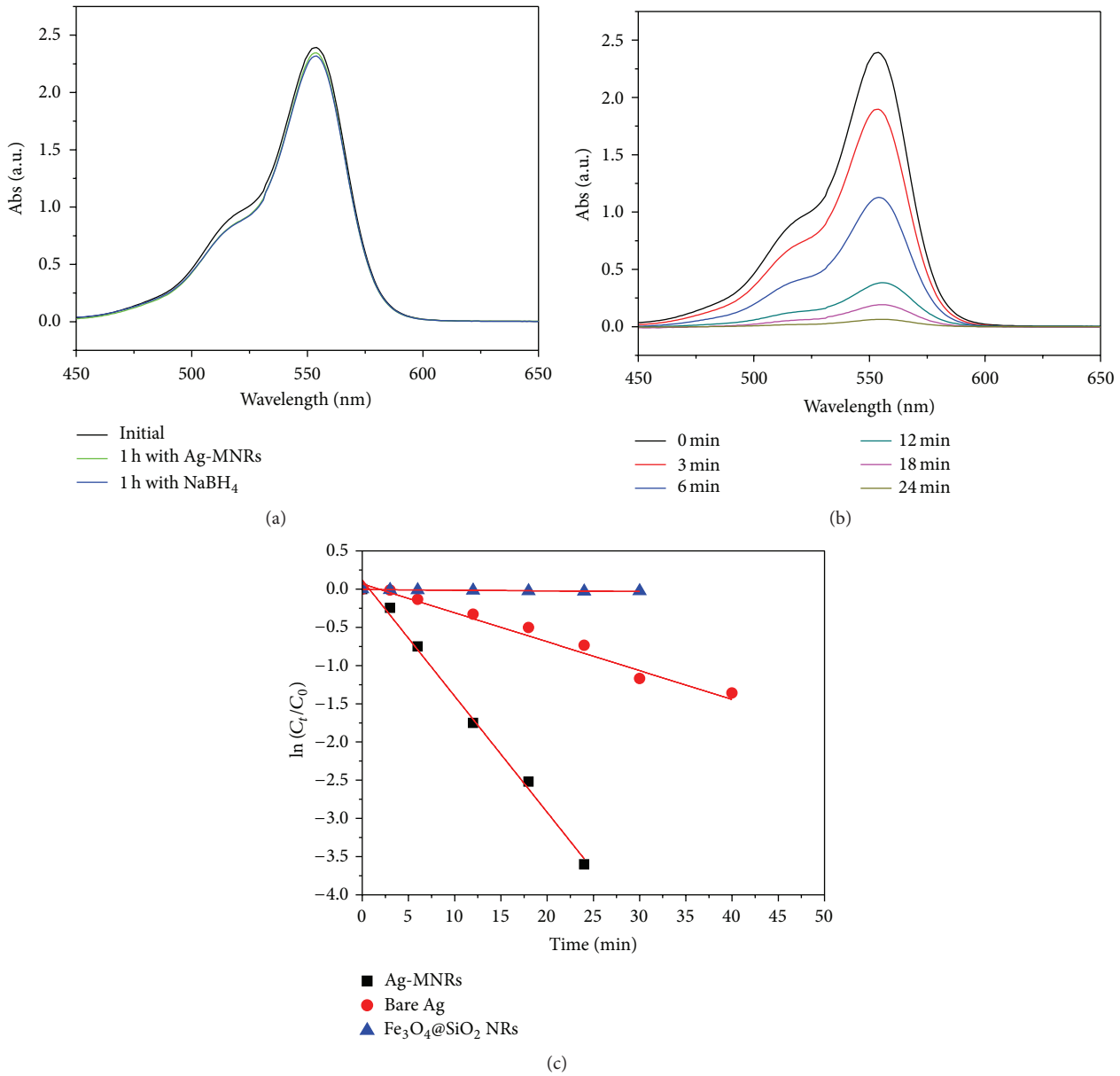

FIGURE 5: Time-dependent UV-Vis absorption spectra for the reduction of RhB by Ag-MNRs (a) in the absence of $NaBH_4$ or Ag-MNRs and (b) in the presence of Ag-MNRs and $NaBH_4$ and (c) kinetic curves for the reduction of RhB catalyzed by Ag-MNRs, bare Ag NPs, and Fe_3O_4@SiO_2 NRs.

The M_s value of Ag-MNRs is lower than that of Fe_3O_4@SiO_2 NRs, which can be ascribed to the decorated nonmagnetic Ag NPs. As the concentration of Fe_3O_4 decreased, the saturation magnetization decreased. Compared with Fe_3O_4 NPs reported previously [8, 12, 13, 29], these as-prepared products show higher coercivity values which are 338 Oe (Fe_3O_4@SiO_2 NRs) and 312 Oe (Ag-MNRs), respectively. This high coercivity may come from the enhanced shape anisotropy of the rod-like structure [30]. The digital photograph inset in Figure 8(a) clearly illustrated the excellent magnetic response of the samples; when placing a magnet near the bottle, the Ag-MNRs catalysts were attracted to the side of the bottle within a few seconds and the solution became transparent, which is facilitative for recycle applications. Figure 8(b) shows the recyclability of the Ag-MNRs catalysts for reduction of RhB; the degradation of RhB was still higher than 80% after five successive cycles, indicating that the Ag-MNRs could be reused without a significant loss of catalytic efficiency.

4. Conclusions

In summary, we have demonstrated a facile step-by-step method to construct Ag nanoparticles decorated Fe_3O_4@SiO_2 nanorods (Ag-MNRs). This method involves coating α-Fe_2O_3 NRs with silica layer and annealed in

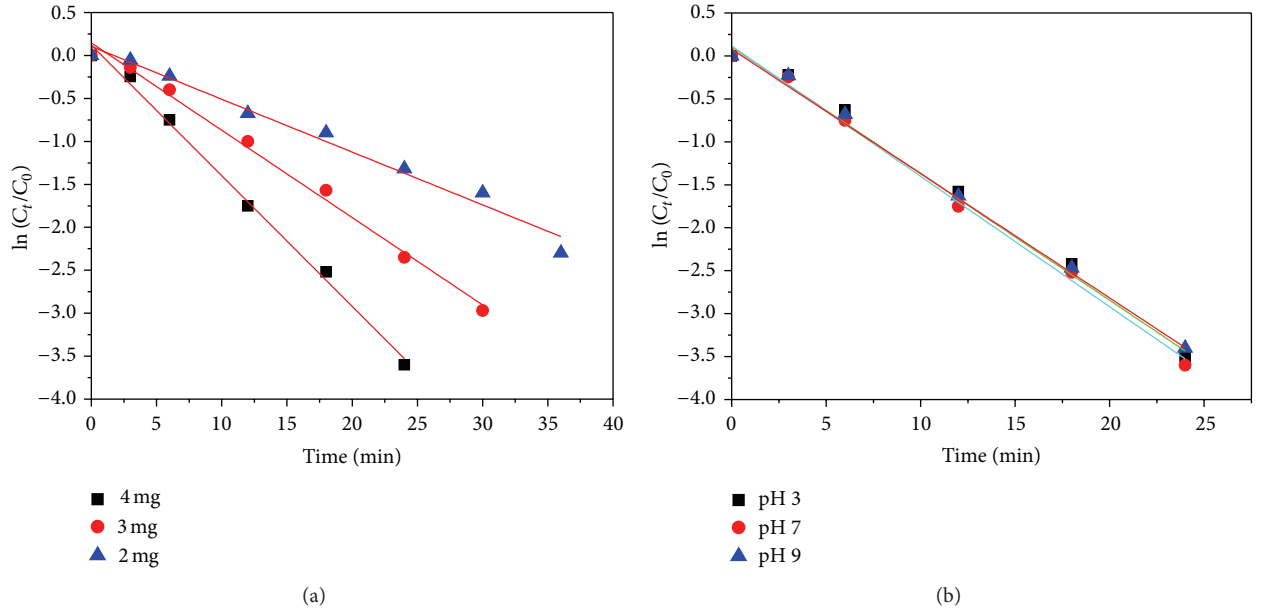

Figure 6: (a) Kinetic curves for the reduction of RhB by Ag-MNRs with different catalyst amounts (pH = 7) and (b) kinetic curves for the reduction of RhB by Ag-MNRs at different pH values (catalyst amounts = 4 mg).

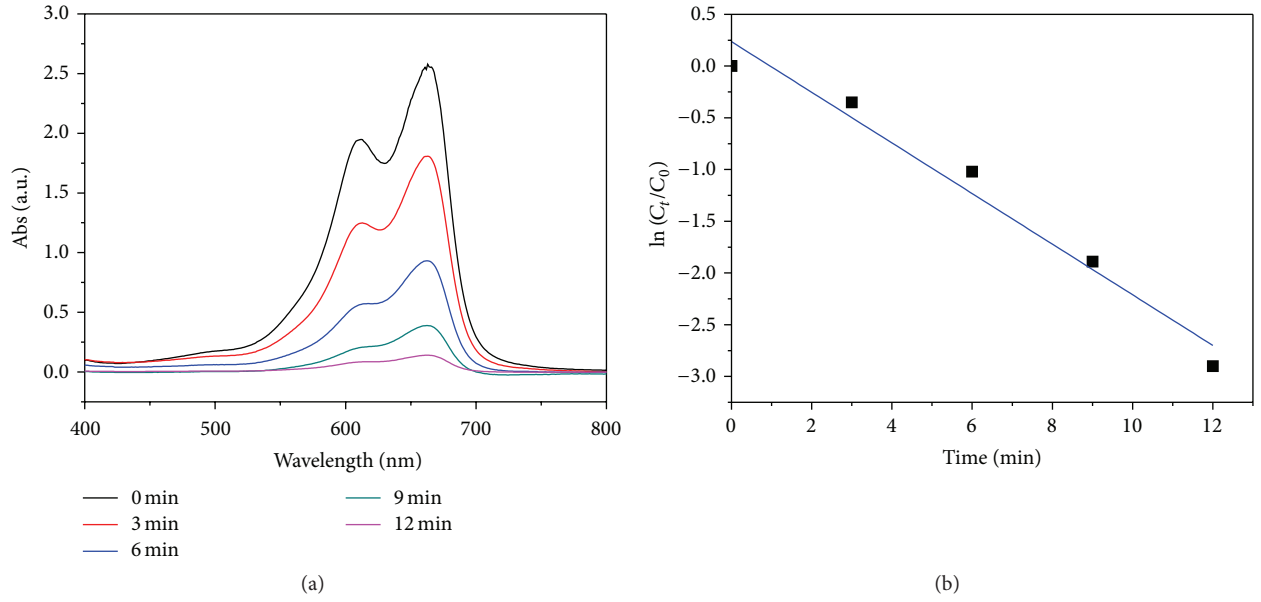

Figure 7: (a) Time-dependent UV-Vis absorption spectra for the reduction of MB by Ag-MNRs and (b) kinetic curves for the reduction of MB by Ag-MNRs.

reduction atmosphere to transform the nonmagnetic α-Fe_2O_3@SiO_2 NRs to magnetic Fe_3O_4@SiO_2 NRs. Then, Ag NPs were deposited on the surface of the Fe_3O_4@SiO_2 NRs by a sonochemical step. These as-prepared Ag-MNRs show superior catalytic ability for the degradation of organic dyes such as RhB and MB. Moreover, the Ag-MNRs catalysts were magnetically separable and still exhibited excellent catalytic performance after at least five cycles, which make them excellent candidates for environmental issues.

Competing Interests

The authors declare that they have no competing interests.

Acknowledgments

This work is funded by the National Basic Research Program of China (Grant no. 2015CB921502), the National Natural Science Foundation of China (Grant nos. 11474184 and

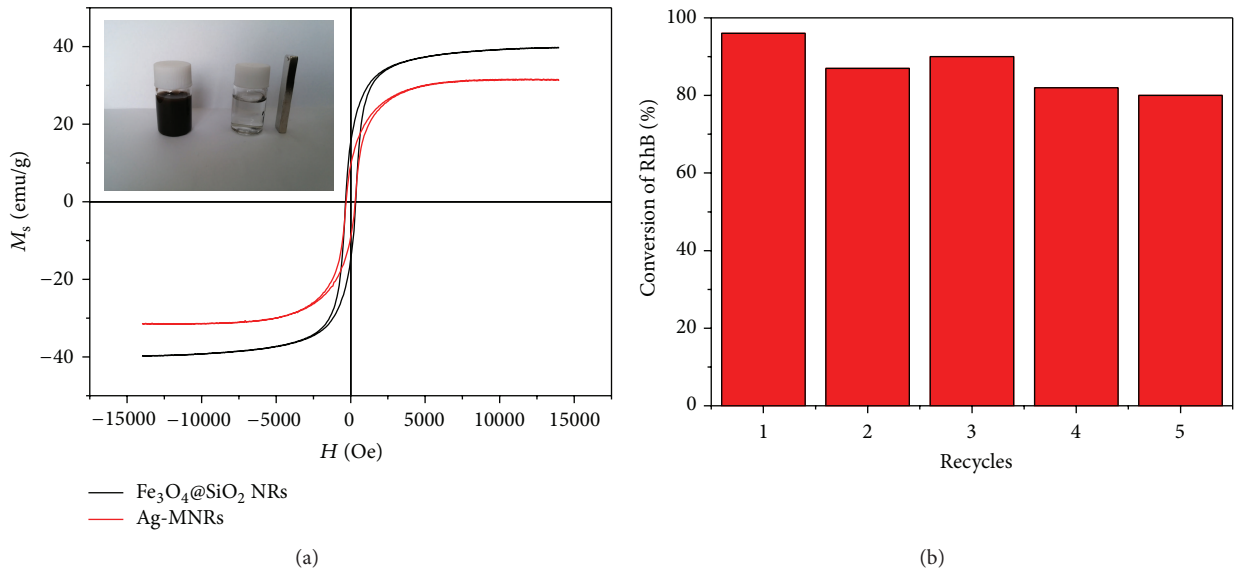

FIGURE 8: (a) Room temperature magnetic curves for Fe_3O_4@SiO_2 NRs (black) and Ag-MNRs (red) and (b) conversion percentage of RhB in five successive reaction cycles with the Ag-MNRs and $NaBH_4$.

11174183), the 111 Project under Grant no. B13029, and The Fundamental Research Funds of Shandong University.

References

[1] I. Ali, "New generation adsorbents for water treatment," *Chemical Reviews*, vol. 112, no. 10, pp. 5073–5091, 2012.

[2] R. Sahoo, A. Roy, C. Ray et al., "Decoration of Fe_3O_4 base material with Pd loaded CdS nanoparticle for superior photocatalytic efficiency," *Journal of Physical Chemistry C*, vol. 118, no. 21, pp. 11485–11494, 2014.

[3] Y. L. Li, Z. Q. Zhang, J. F. Shen, and M. X. Ye, "Hierarchical nanospheres based on Pd nanoparticles dispersed on carbon coated magnetite cores with a mesoporous ceria shell: a highly integrated multifunctional catalyst," *Dalton Transactions*, vol. 44, no. 37, pp. 16592–16601, 2015.

[4] Y. J. Xie, B. Yan, H. L. Xu et al., "Highly regenerable mussel-inspired Fe_3O_4@polydopamine-Ag core-shell microspheres as catalyst and adsorbent for methylene blue removal," *ACS Applied Materials and Interfaces*, vol. 6, no. 11, pp. 8845–8852, 2014.

[5] T. Zhang, X. Li, S.-Z. Kang, L. Qin, G. Li, and J. Mu, "Facile assembly of silica gel/reduced graphene oxide/Ag nanoparticle composite with a core-shell structure and its excellent catalytic properties," *Journal of Materials Chemistry A*, vol. 2, no. 9, pp. 2952–2959, 2014.

[6] D. Wang and Y. Li, "One-pot protocol for au-based hybrid magnetic nanostructures via a noble-metal-induced reduction process," *Journal of the American Chemical Society*, vol. 132, no. 18, pp. 6280–6281, 2010.

[7] U. Kurtan, M. Amir, and A. Baykal, "Fe_3O_4@Nico-Ag magnetically recyclable nanocatalyst for azo dyes reduction," *Applied Surface Science*, vol. 363, no. 1-2, pp. 66–73, 2016.

[8] J. Ma, S. Guo, X. Guo, and H. Ge, "ZrO_2@Ag composite catalyst for hydrogenation reduction of organic dye: preparation and characterization as well as catalytic performance evaluation," *Ceramics International*, vol. 41, no. 9, pp. 12453–12458, 2015.

[9] L. H. Ai, H. T. Yue, and J. Jiang, "Environmentally friendly light-driven synthesis of Ag nanoparticles *in situ* grown on magnetically separable biohydrogels as highly active and recyclable catalysts for 4-nitrophenol reduction," *Journal of Materials Chemistry*, vol. 22, no. 44, pp. 23447–23453, 2012.

[10] S. C. Tang, S. Vongehr, Z. Zheng, H. J. Liu, and X. Meng, "Silver doping mediated route to bimetallically doped carbon spheres with controllable nanoparticle distributions," *Journal of Physical Chemistry C*, vol. 114, no. 43, pp. 18338–18346, 2010.

[11] J. Zheng, Y. Dong, W. Wang et al., "In situ loading of gold nanoparticles on Fe_3O_4@SiO_2 magnetic nanocomposites and their high catalytic activity," *Nanoscale*, vol. 5, no. 11, pp. 4894–4901, 2013.

[12] P. S. Rathore, R. Patidar, and S. Thakore, "Nanoparticle-supported and magnetically recoverable organic–inorganic hybrid copper(II) nanocatalyst: a selective and sustainable oxidation protocol with a high turnover number," *RSC Advances*, vol. 4, no. 77, pp. 41111–41121, 2014.

[13] A. Bayat, M. S. Fard, N. Ehyaei, and M. M. Hashemi, "Silver nanoparticles supported on silica-coated ferrite as magnetic and reusable catalysts for oxidant-free alcohol dehydrogenation," *RSC Advances*, vol. 5, no. 29, pp. 22503–22509, 2015.

[14] Y. Yu, M.-Z. Zhang, J. Chen, and Y.-D. Zhao, "Homogeneous synthesis of SiO_2@TiO_2 nanocomposites with controllable shell thickness and their enhanced photocatalytic activity," *Dalton Transactions*, vol. 42, no. 4, pp. 885–889, 2013.

[15] C. G. Hu, X. Q. Zhai, Y. Zhao et al., "Small-sized PdCu nanocapsules on 3D graphene for high-performance ethanol oxidation," *Nanoscale*, vol. 6, no. 5, pp. 2768–2775, 2014.

[16] Z. W. Zhang, Y. M. Zhou, Y. W. Zhang et al., "A highly reactive and magnetic recyclable catalytic system based on AuPt nanoalloys supported on ellipsoidal Fe@SiO_2," *Journal of Materials Chemistry A*, vol. 3, no. 8, pp. 4642–4651, 2015.

[17] S. Singh and D. Bahadur, "Catalytic and antibacterial activity of Ag decorated magnetic core shell nanosphere," *Colloids and Surfaces B: Biointerfaces*, vol. 133, pp. 58–65, 2015.

[18] M. Abbas, S. R. Torati, and C. Kim, "A novel approach for the synthesis of ultrathin silica-coated iron oxide nanocubes decorated with silver nanodots ($Fe_3O_4SiO_2$/Ag) and their superior catalytic reduction of 4-nitroaniline," *Nanoscale*, vol. 7, no. 28, pp. 12192–12204, 2015.

[19] C.-J. Jia, L.-D. Sun, Z.-G. Yan et al., "Single-crystalline iron oxide nanotubes," *Angewandte Chemie—International Edition*, vol. 44, no. 28, pp. 4328–4333, 2005.

[20] S. Gai, P. Yang, C. Li et al., "Synthesis of magnetic, up-conversion luminescent, and mesoporous core–shell-structured nanocomposites as drug carriers," *Advanced Functional Materials*, vol. 20, no. 7, pp. 1166–1172, 2010.

[21] M. Kumar and S. Deka, "Multiply twinned AgNi alloy nanoparticles as highly active catalyst for multiple reduction and degradation reactions," *ACS Applied Materials and Interfaces*, vol. 6, no. 18, pp. 16071–16081, 2014.

[22] S. C. Tang, S. Vongehr, and X. K. Meng, "Controllable incorporation of Ag and Ag-Au nanoparticles in carbon spheres for tunable optical and catalytic properties," *Journal of Materials Chemistry*, vol. 20, no. 26, pp. 5436–5445, 2010.

[23] M. Xiao, C. Zhao, H. Chen, B. Yang, and J. Wang, "'Ship-in-a-bottle' growth of noble metal nanostructures," *Advanced Functional Materials*, vol. 22, no. 21, pp. 4526–4532, 2012.

[24] H.-L. Jiang, T. Akita, T. Ishida, M. Haruta, and Q. Xu, "Synergistic catalysis of Au@Ag core−shell nanoparticles stabilized on metal−organic framework," *Journal of the American Chemical Society*, vol. 133, no. 5, pp. 1304–1306, 2011.

[25] Y. Zhang, P. Zhu, L. Chen et al., "Hierarchical architectures of monodisperse porous Cu microspheres: synthesis, growth mechanism, high-efficiency and recyclable catalytic performance," *Journal of Materials Chemistry A*, vol. 2, no. 48, pp. 11966–11973, 2014.

[26] P. H. Zhang, Y. M. Sui, G. J. Xiao et al., "Facile fabrication of faceted copper nanocrystals with high catalytic activity for p-nitrophenol reduction," *Journal of Materials Chemistry A*, vol. 1, no. 5, pp. 1632–1638, 2013.

[27] L. Ai, C. Zeng, and Q. Wang, "One-step solvothermal synthesis of Ag-Fe_3O_4 composite as a magnetically recyclable catalyst for reduction of Rhodamine B," *Catalysis Communications*, vol. 14, no. 1, pp. 68–73, 2011.

[28] X. Du, J. He, J. Zhu, L. Sun, and S. An, "Ag-deposited silica-coated Fe_3O_4 magnetic nanoparticles catalyzed reduction of p-nitrophenol," *Applied Surface Science*, vol. 258, no. 7, pp. 2717–2723, 2012.

[29] T. Yao, T. Cui, H. Wang, L. Xu, F. Cui, and J. Wu, "A simple way to prepare Au@polypyrrole/Fe_3O_4 hollow capsules with high stability and their application in catalytic reduction of methylene blue dye," *Nanoscale*, vol. 6, no. 13, pp. 7666–7674, 2014.

[30] X. Y. Zhang, G. H. Wen, Y. F. Chan, R. K. Zheng, X. X. Zhang, and N. Wang, "Fabrication and magnetic properties of ultrathin Fe nanowire arrays," *Applied Physics Letters*, vol. 83, no. 16, pp. 3341–3343, 2003.